LANGMUIR Article
Cite This: Langmuir 2019, 35, 5029−5036
pubs.acs.org/Langmuir

ReaxFF MD Simulations of Peptide-Grafted Gold Nanoparticles

Mohammadreza Samieegohar,[†] Feng Sha,[‡] Andre Z. Clayborne,[§] and Tao Wei*[,†]

[†]Chemical Engineering Department, Howard University, 2366 Sixth Street, Washington, District of Columbia 20059, United States
[‡]Network Information Center, Xiamen University of Technology, 600 Ligong Road, Jimei District, Xiamen 361024, Fujian Province, China
[§]Chemistry Department, Howard University, 525 College Street, Washington, District of Columbia 20059, United States

Supporting Information

ABSTRACT: Functionalized gold nanoparticles have critical applications in biodetection with surface-enhanced Raman spectrum and drug delivery. In this study, reactive force field molecular dynamics simulations were performed to study gold nanoparticles, which are modified with different short-chain peptides consisting of amino acid residues of cysteine and glycine in different grafting densities in the aqueous environment. Our study showed slight facet-dependent peptide adsorption on a gold nanoparticle with the 3 nm core diameter. Peptide chains prefer to adsorb on the Au(111) facet compared to those on other facets of Au(100) and Au(110). In addition to the stable thiol interaction with gold nanoparticle surfaces, polarizable oxygen and nitrogen atoms show strong interactions with the gold surface and polarize the gold nanoparticle surfaces with an overall positive charge. Charges of gold atoms vary according to their contacts with peptide atoms and lattice positions. However, at the outmost peptide layer, the whole functionalized Au nanoparticles exhibit overall negative electrostatic potential due to the grafted peptides. Moreover, simulations show that thiol groups can be deprotonated and subsequently protons can be transferred to water molecules and carboxyl groups.

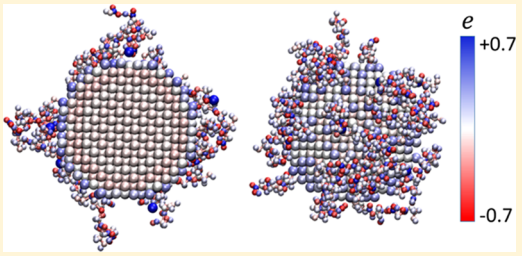

INTRODUCTION

Gold nanoparticles (AuNPs) have been extensively studied due to their size-dependent electronic,[1] biocompatible,[2] nontoxic,[3] and optical properties.[4] These qualities make AuNPs an ideal candidate for optical detection agents,[5] diagnostics,[6] nanotherapeutics,[7] and drug delivery systems.[8] The plasmonic response of AuNPs, e.g., surface-enhanced Raman spectrum, is critical for molecular detection. The extremely intense localized electromagnetic fields render AuNPs to act as sensitive transducers of small changes in the local refractive index upon organic molecular adsorption, leading to localized surface plasmon resonance spectrum shifts of extinction and scattering spectra. Density functional theory (DFT) studies[9] showed that the spectra shifts observed for a ligated small-sized gold nanoparticle (i.e., a cluster of 25 gold atoms) can be attributed to the geometric distortions in the core lattice and ultimately to changes in the electronic structure, with respect to a change in the ligand composition. Raman experiments[10] demonstrated that upon alkanethiol adsorption, a linear red shift of 3.0 nm for the peak extinction wavelength is detected for every carbon atom in the alkane chain and a blue shift of 8.5 nm due to the Ag−S charge transfer. AuNP surfaces can be easily functionalized with a wide range of biofunctional molecules, which contain thiol groups.[11] In drug delivery, thiol−gold interactions provide the opportunity to synthesize novel hybrid materials such as peptide-grafted AuNPs. The peptides utilized in these systems can fulfill different roles, acting as drug carriers, anticancer drugs, and even cellular targeting moieties.[12] Luminescent AuNPs of less than 3.0 nm, coated with zwitterionic glutathione, which is composed of amino acid residues of cysteine (C), glycine (G), and glutamate (E), were found to have efficient renal clearance and antibiofouling for broad preclinical applications in cancer diagnosis and kidney functional imaging.[13] AuNPs coated with peptides of CGCG show the characteristic plasmon absorption bands ($\lambda_{max} \sim 514$ nm) in the UV−visible spectra.[14]

Extensive studies[9,13−20] have been conducted to examine the nature of Au−peptide interactions and the stability of self-assembled peptide monolayers (SAMs) formed on gold surfaces under various conditions. Peptides are capable of having chemisorption onto AuNP surfaces due to strong thiolate−Au bonds.[17,18] Au−S binding mode shifts from a coordinate bond to a covalent bond as the environmental pH increases.[15] Recent experiments,[13] which compared AuNPs coated with cysteine and with glycine−cysteine amino acid residues, showed that introducing an additional glycine residue can significantly enhance the physiological stability of zwitterionic AuNPs and improve their resistance to serum proteins. Infrared and NMR measurements showed that for AuNPs coated with cysteine/glycine-containing peptides in the aqueous environment the backbone conformation and hydro-

Received: November 26, 2018
Revised: February 21, 2019
Published: March 14, 2019

DOI: 10.1021/acs.langmuir.8b03951
Langmuir 2019, 35, 5029−5036

gen-bonding pattern of the conjugated peptides undergo significant changes due to peptide−gold surfaces' interactions.[14] In addition to strong thiol−gold interactions, polarizable atoms in peptide molecules can bind epitaxial sites of nonoxidized metal surfaces.[19,20] Moreover, the peptide adsorption to Au(111) surface was found to be thermodynamically favored over other facets, e.g., Au (100) in an aqueous solution, as a result of different adsorption free energy.[18−20]

Computer simulations have also been performed to study biomolecular interfacial behavior. Simulation methods, such as conventional molecular dynamics (MD),[21−32] Monte Carlo,[33,34] and discrete molecular dynamics[35,36] simulations, focus on the physical nonbonding interactions while neglecting possible chemical reactions, e.g., ionizable groups' protonation/deprotonation equilibrium and thiol−Au interactions and chemisorption. The development of the reactive force field (ReaxFF),[37] as a polarizable charge model based on the bond order, has made it possible to simulate chemical reactions, including combustion,[38,39] hydrocarbon pyrolysis,[40,41] thermal decomposition of polymers,[42] the explosion of high-energy materials,[43,44] and the oxidation of solid surfaces[45] and NPs.[46] By allowing chemical bonds to form and break freely without fixing the rigid connectivity between atoms inside a molecule or fixing atoms' partial charges, ReaxFF MD overcomes the deficiencies of conventional MD and the scale problem of quantum mechanics.[9,47] A recent study employed ReaxFF MD to study biomolecules, e.g., short peptides and small proteins in water.[48] To date, the reported ReaxFF MD parameters are available for three amino acids (cysteine, glycine, and alanine) interacting with the gold surface.[48−50] Simulations showed that the cysteine adsorption process consists of the initial slow physisorption of cysteine molecules onto the gold surface and subsequent fast chemisorption, which is highly correlated with the specific orientation and location of cysteine/cystine on the substrate surfaces.[50−52]

In molecular detection using SERs, the detector, which contains an array of NPs in quantum size range (diameter < 10 nm), has a significant blue shift of the plasmon resonance due to the smearing of electronic charge distribution over the particle's surface.[53] In addition, in drug delivery, a particle's size is limited to a scale smaller than the size of a nuclear pore of 9−12 nm.[54] To this end, this work focused on small-sized AuNPs with 3.0 nm diameter for the nanoparticle's core to study their interactions with short peptide chains (CGCG and CGGG) of different surface densities in water, using ReaxFF MD simulations. Peptides containing cysteine and glycine amino acid residues play an important role in stabilizing gold nanoparticles in the applications of biomedical imaging[13] and targeting biomarker.[14] In our work, several critical questions are addressed regarding peptide interactions with AuNP surfaces, possible facet-dependent adsorption, AuNP surface polarization, the charge distribution of the whole nanoparticle, and possible peptides' protonation/deprotonation reactions around AuNPs. These fundamental studies will pave the way for the future development of SERs for biomolecule detection and drug delivery technologies using functionalized AuNPs. The rest of the article is organized as follows: the section of Method provides details of the implementation of ReaxFF simulations; the section of Results presents our simulation results; and the article then concludes with a summary in the section of Conclusions.

METHOD

ReaxFF MD simulations were performed using the software package of large-scale atomic/molecular massively parallel simulator (LAMMPS)[55] (version released on November 17, 2016) with parameters taken from the literature.[50] The structure of a bare gold nanocrystal without ligands, named AuNP bare, is obtained by cutting a nearly spherical nanocrystal out of a bulk face-centered cubic structure gold lattice. The core of AuNP (i.e., AuNP bare), with a 3 nm diameter, consists of 1464 atoms with 6 Au(100) facets, 8 Au(111) facets, and 12 Au(110) facets (Figure 1). To optimize

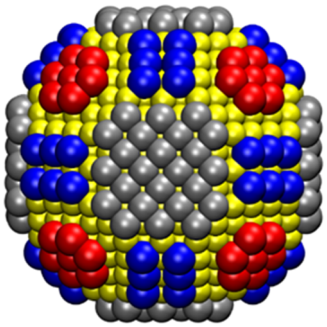

Figure 1. Gold nanoparticle core (red: the outer layer of Au(111) facet, silver: the outer layer of Au(100) facet, blue: the outer layer of Au(110), yellow: inner Au layers).

the bare AuNP structure, an NP was inserted in a water cubic box (length = 6 nm) with periodic boundary condition (PBC). The system was first relaxed for 100 ps in the NVT assemble with annealing process (5−289.15 K) before modifying the NP surfaces with peptide chains. The short chains of peptides (CGCG and CGGG) were used to graft gold nanoparticles through cysteine−thiol interactions with Au nanoparticle surfaces.[56] The purpose of using different types of peptides (CGCG and CGGG) is to investigate the polarization and interactions of peptides with AuNPs, as well as the thiol−AuNP interactions. AuNPs were decorated with 47 and 72 chains of peptides, corresponding to surface densities of 1.46 peptides/nm^2 and 2.24 peptides/nm^2, which are in the range of previous experimental and theoretical investigations of functional AuNPs[56,58,59] AuNPs grafted with CGCG and CGGG were solvated in two cubic water boxes of lengths 8.72 nm and 8.92 nm, respectively. The three-dimensional periodic boundary condition (PBC) was applied in all directions. All simulation systems were first relaxed for 100 ps in the vacuum at a low temperature of 5 K and heated gradually from temperatures of 100 K to the target temperature of 289.15 K. The whole system was then solvated and relaxed using the same heating protocol. A Berendsen thermostat[57] with a damping constant of 100 fs was employed in the simulation, and a time step of 0.1 fs was adopted. Simulations were performed in the NVT ensemble. ReaxFF describes dynamic charge transfer between atoms based on the charge equilibration (QEq) method,[58,59] which minimizes the electrostatic energy based on the electronegativity and the stiffness parameters. In this work, atomic charges were updated every 10 MD steps using QEq method. The bond order and nonbonded cutoff radii were 0.3 and 10 Å, respectively. Hydrogen bonding and near-neighbor cutoff distances were kept at 0.75 and 0.5 nm, respectively. The atoms' position, bonds, and velocity were collected every 100 fs. The reaction

DOI: 10.1021/acs.langmuir.8b03951
Langmuir 2019, 35, 5029−5036

mechanisms were extracted from the dynamic trajectories of atoms and their bonds. To validate ReaxFF simulations, coarse-grained MD simulations with MARTINI force field parameters[60,61] were also employed for the same systems.

RESULTS

Peptide Adsorption on Gold Nanoparticle Surfaces. We first analyzed the effect of peptide grafting density and AuNP surface orientation on NPs' SAMs morphology, which is highly correlated with NPs' functionality. Figure 2a shows the

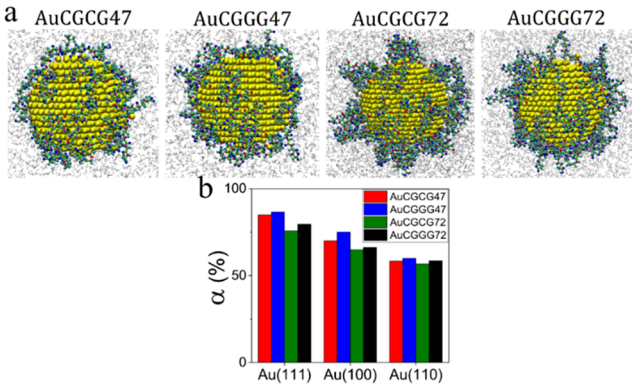

Figure 2. (a) Peptides' surface configurations for different AuNPs: AuCGCG47, AuCGGG47, AuCGCG72, and AuCGGG72; and (b) normalized surface coverages (α) for surface orientations.

peptide structure on the surface of four AuNPs, which are grafted with peptide chains of CGCG and CGGG at different surface grafting densities after simulations of 0.7−1.0 ns. The gyration radii of functionalized AuNPs of the four systems are $r_{AuCGCG47}$ = 2.13 nm, $r_{AuCGGG47}$ = 2.07 nm, $r_{AuCGCG72}$ = 2.48 nm, and $r_{AuCGGG72}$ = 2.41 nm, respectively. The results show that in the cases of low-density, 1.46 peptides/nm^2 (AuCGCG47 and AuCGGG47), peptide chains are adsorbed on AuNPs' surface more tightly than chains of the high-density, 2.24 peptides/nm^2 (AuCGCG72 and AuCGGG72). Compared with NPs at a lower surface density, due to the steric effect and interchain interactions, the peptide chains form extended mushroom-shaped conformations on the NP surfaces of high packing density. It should also be noted that in the range of grafting densities of our simulations the difference of gyration radius for NPs, which are modified with different peptide chains (CGCG and CGGG), is negligible. As discussed next, besides sulfur atoms, the polarizable atoms of oxygen and nitrogen display strong binding onto AuNP surfaces, and the crowded peptide chains adjacent to the AuNP surfaces generate steric effect to prevent cysteine residues from interacting with the gold surfaces, possibly leading to a long relaxation time scale beyond our simulation length. To validate ReaxFF simulations, we also performed coarse-grained MD simulations. Both ReaxFF and CG MD simulations show similar values of gyration radius for the same peptide-grafted gold nanoparticles, which validates that the short peptide chains (AuCGCG47) around gold nanoparticles have been relaxed in ReaxFF simulations (Figure S4).

To examine the effect of the nanoparticle's facet on peptide−gold interactions, the normalized surface coverage (α) of peptide atoms for a AuNP facet orientation was used

$$\alpha = \frac{N_{ads}}{N_i} \times 100\% \quad (1)$$

where N_{ads} is the number of peptide atoms within the distance of 3 Å from the AuNP surfaces and N_i represents the total atom number of the outermost layer of the gold surface for a specific facet (i.e., Au(111), Au(100), or Au(110)). A comparison of the facets of different orientations shows that nanoparticles of a low grafting density have a higher value of α, which confirms our previous observation that at lower surface density more peptide atoms are on the NP surface. The analysis of the normalized surface coverage (α) also indicates slight facet-dependent adsorption. Despite the initial even distribution of grafted peptides on the AuNP surface (Figure S1 in the Supporting Information), the Au(111) facet has the largest total number of peptide atoms as compared to the Au(100) and Au(110). Previous research similarly showed that peptides adsorb more strongly on Au(111) surfaces than on other facets, due to the number of the metal surface' epitaxial contacts per molecule, the atoms' polarizability, and the precision of the geometric fit.[19,20,62]

Figure 3a shows the conformation of the AuCGCG47 nanoparticle after 0.74 ns simulations in water as an example to

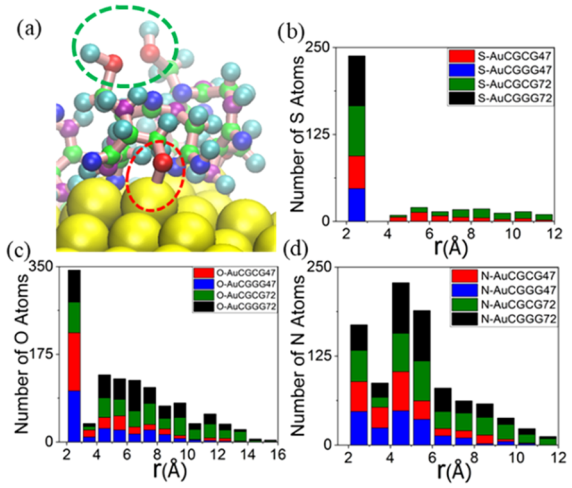

Figure 3. (a) Snapshot of AuCGCG47 NP (Au atoms: yellow, S atoms: red, H atoms: cyan, O atoms: blue, N atoms: purple, C atoms: green); (b) histogram of sulfur atoms' distance to AuNP surfaces; (c) histogram of oxygen atoms' distance to AuNP surfaces; and (d) histogram of nitrogen atoms' distance to AuNP surfaces.

illustrate sulfur atoms' distribution on the AuNP surface. In our simulation, short peptide chains were grafted onto the gold nanoparticle surfaces through thiol−Au interactions. The sulfur atoms of terminal cysteine groups of peptide chains display stable thiol−Au interactions during the course of simulations (Figure 3a). However, other sulfur atoms that reside in the middle of the peptide chain away from the nanoparticle surfaces show minimal-to-no interactions with the nanoparticle surface. This can be attributed to the steric effects, resulting from the crowed grafted peptide chains (Figure 3a). To further quantify the distribution of peptide atoms around a AuNP, proximal radial distribution criteria[24] were used, where the distances of sulfur atoms of peptide chains to all gold atoms were calculated and their minimum value was chosen as its distance to the AuNP surface. The final 100 configurations spanning the last 100 ps were used to obtain the averaged

DOI: 10.1021/acs.langmuir.8b03951
Langmuir 2019, 35, 5029−5036

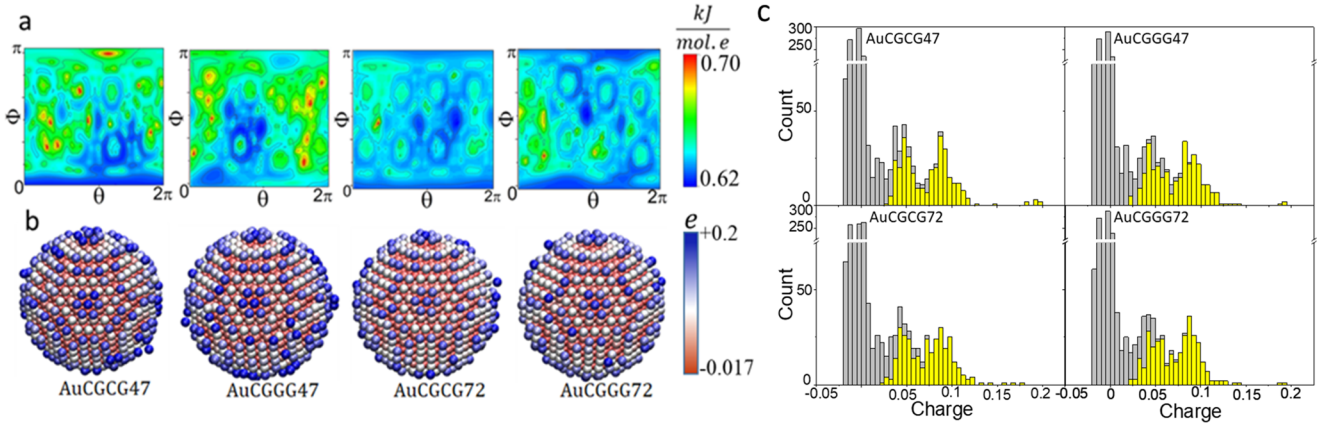

Figure 4. (a) Contour of electrostatic potential (E) as a function of spherical angles (ϕ and θ) at r = 1.8 nm; (b) charge distribution on the AuNP core. The origin of the spherical coordinate is the center of a AuNP; and (c) histogram of the image charges of gold atom distribution.

surface distance. Figure 3b shows the histograms for the distribution of all sulfur atoms for different nanoparticles (AuCGCG47, AuCGGG47, AuCGCG72, and AuCGGG72). It is observed that there is a layer of sulfur atoms on the AuNP surface with an average binding distance of 2.45−2.46 Å, which is within the range of Au−S distance in chemisorption,[63,64] whereas other unbounded sulfur atoms are distributed in the region away from the nanoparticle's surfaces. The sulfur atoms in the binding layer (Au−S) were more stable than those away from the AuNP surfaces, as shown in the root-mean-square displacement (RMSD) profiles (Figure S2). Similarly, previous NMR experiments[65] revealed that cysteine residues form two layers on the AuNP surfaces, where the inner layer is composed of cysteine molecules chemisorbed to the gold surface and the outer layers interact with the bulk and atoms of the inner layer. Our results demonstrated that the method of ReaxFF simulations and the force field parameters adopted can present the thiol−Au interactions.

Using the same protocol, the distribution of oxygen atoms' distance to AuNP surfaces was analyzed with a histogram (Figure 3c). The results indicate that the interaction distances of Au and oxygen atoms can be categorized into two different levels. At the first level, for all four NPs, oxygen atoms are bound onto the AuNP surfaces via an average interacting distance of 2.1 Å. In consistence with this finding, previous DFT simulations[66] illustrated that in the presence of water molecules glycine adsorbs on gold surfaces with a Au−O bond distance of 2.317 Å, which can be attributed to their strong binding on gold surfaces. Our results show that at the second level the oxygen atoms are located away from the surfaces. The nitrogen atoms also exhibit a two-level distribution around the AuNP surfaces, although their distribution is more uniform compared to oxygen atoms (Figure 3d). On different AuNP surfaces, the Au−N bonding distance is 2.4 Å, close to the previous DFT computational value[64] of 2.35 Å, which indicates that N atoms participate in the molecule−substrate coupling. It is also noteworthy that our results show more O−Au and N−Au interactions in cases of lower grafting density (AuCGCG47 and AuCGGG47) than in high grafting density cases (AuCGCG72 and AuCGGG72). These results are consistent with those of normalized surface coverage and gyration radius mentioned above. The steric effect that arises from the packed polymeric layer on AuNP surfaces hinders the contacts of polarizable sulfur, oxygen, and nitrogen atoms, which locate away from the terminals of peptide chains.

Electrostatic Potential of the AuNPs. To characterize the AuNP surfaces' charge distribution as a result of polarization and charge transfer upon peptide adsorption, the electrostatic potential (E) resulting from gold atoms' charges of a AuNP nanoparticle core was computed using the protocol in our previous research[67]

$$E(\vec{r}) = 138.935 \sum_{i}^{N} \frac{q_i}{|\vec{r} - \vec{r}_i|} \tag{2}$$

where $E(\vec{r})$ kJ/(mol e) is the electrostatic potential at a radial direction, $\vec{r}$ by summing up the electrostatic interactions over all AuNP atoms; q_i is the charge of an atom, i; and N is the total atom number. Figure 4 shows a contour of the electrostatic potential, E, from gold atoms' charges, including the image charges, as a function of angles (ϕ and θ) at a fixed radius distance, r = 1.8 nm, in the spherical coordinate.

As illustrated in the previous section, for the AuNPs of the lower grafting density (AuCGCG47 and AuCGGG47), more polarizable atoms, i.e., sulfur, oxygen, and nitrogen, locate adjacent to the NP surface. These neighboring atoms introduce more pronounced electrostatic potential on the AuNP surfaces of low surface grafting density, compared with the NPs of high grafting density (AuCGCG72 and AuCGGG72). Another observation is that the electrostatic potential and charge distribution above the NP surface are inhomogeneous (Figure 4a,b) due to the segregation of peptide chains and slight facet-dependent adsorption (Figure 2). Similar to the previous DFT simulations[9] for small gold nanoclusters, our ReaxFF simulations show that the surface of the larger-sized AuNP core has a positive charge distribution, whereas atoms of the inner core display negative charges (Figure 4b). The histogram analysis of the charge distribution for all gold atoms (Figure 4c) shows that on the NP surface, gold atoms thiolate-bound or adsorbed with oxygen and nitrogen have larger positive charges (~0.09e) than other surface atoms (~0.05e) (Figure 4b). The internal core atoms have a small negative charge (~−0.02e). This illustrates that the gold atoms interacting directly with the peptide lose some amount of charge. In addition, our simulations show that individual gold atoms can separate from the gold nanoparticle's surfaces (Figure 4b), being polarized with larger positive charges (Figure 4c). Interestingly, these results show a consistent pattern similar to that of smaller-sized (diameter < 3 nm) gold nanoparticles interacting with thiol ligands.[65,68,69]

DOI: 10.1021/acs.langmuir.8b03951
Langmuir 2019, 35, 5029−5036

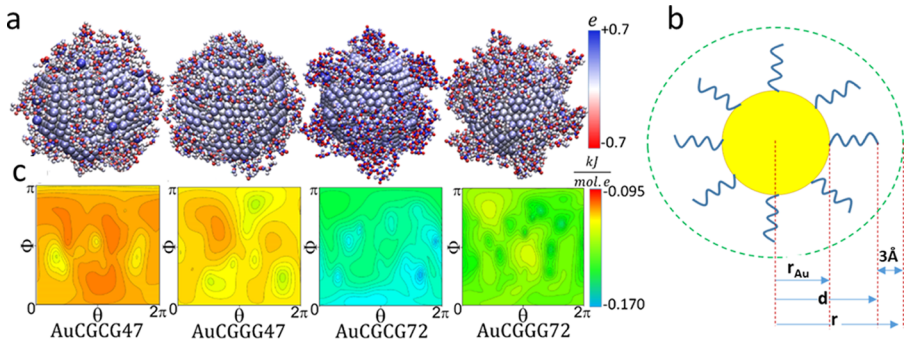

Figure 5. (a) Charge distribution of functionalized AuNPs; (b) schematic graph of a functionalized AuNP (r_{Au} (=1.5 nm) is the radius of the AuNP core, d: the maximum thickness of peptides on the AuNP surface determined from peptide density profiles, r (=d + 3 Å): the position to calculate the electrostatic potential, $E(\vec{r})$); (c) contour of $E(\vec{r})$ as a function of spherical angles (ϕ and θ) at $r_{AuCGCG47}$ = 3.33 nm, $r_{AuCGGG47}$ = 3.39 nm, $r_{AuCGCG72}$ = 3.52 nm, $r_{AuCGGG72}$ = 3.55 nm. The origin of the spherical coordinate is the center of a AuNP.

Further investigation into the accuracy of the polarization, particularly in an aqueous environment, will be reported in our future publication using an improved polarizable QEq method, called ReaxPQ+,[70] which has recently been proposed based on a core−shell charge and implemented in the open source code of RXMD (ReaxFF reactive molecular dynamics). The exterior Au atoms typically have a slightly positive charge due to the interactions of the thiol ligands with the exterior atoms.[69] The overall charges of AuNP cores for the cases of low grafting packing density (AuCGCG47 and AuCGGG47) are more positive than those of high grafting density (AuCGCG72 and AuCGGG72). This observation is consistent with the number of peptide atoms adsorbed on NP surfaces, as illustrated in the previous section (see Figure 3c). Also, the nanoparticles grafted with peptides of CGCG have slightly more positive charges than the NPs grafted with peptides of CGGG.

Next, the electrostatic potential on the outer surface of the whole functionalized NP was examined (Figure 5). Previous experimental investigations[71−73] showed that the charges of the nanoparticle outer surfaces have a profound effect on the nanoparticle's circulation and cellular uptake. In this work, peptides composed of amino acid residues of glycine and cysteine were chosen to study their electrostatic potential around a gold surface. The purpose of using ReaxFF MD simulations is to take into account the factors of polarization, charge transfer, and the protonation states of amino acid residues more precisely compared with conventional MD simulations, where atomic charges are fixed and chemical bonds cannot be altered. Figure 5a shows the distribution of atomistic charges of the whole functionalized AuNPs. The grafting peptides (CGCG and CGGG) around AuNP surfaces are with negative charges. Therefore, they induce a total positive charge on the AuNP surface, as demonstrated above. Figure 5c shows a contour of the electrostatic potential, E, as a function of angles (ϕ and θ) at a radial distance, which is 0.3 nm more than the maximum radius, chosen based on peptide density profiles (Figures 5b and S4 in the Supporting Information). The results show that the electrostatic potentials of the whole functionalized AuNPs have negative values in the range from −0.095 to −0.170 kJ/(mol e), which is close to experimental values.[13] Figure 5c shows for AuNPs of high grafting density (AuCGCG72 and AuCGGG72) that their surfaces exhibit more negative electric potential compared to NPs of lower grafting density (AuCGCG47 and AuCGGG47).

Protonation/Deprotonation of Peptides on AuNP Surfaces. Near the surface of an NP, the local pH can be different from that in the bulk solution due to local interactions in the local polymeric environment of SAMs and the interactions with the core of nanoparticles. Subsequently, amino acid residues of peptides can display various protonation states at the NP interface. Our ReaxFF MD simulations show that thiol groups from amino residues of cysteine can alter their protonation states (Figure 6a). From

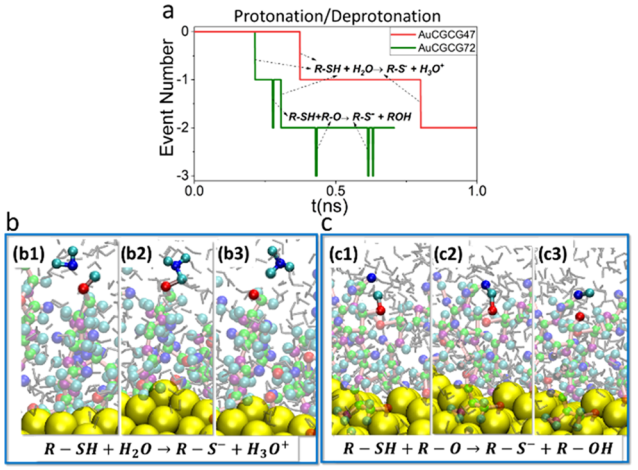

Figure 6. (a) Protonation/deprotonation of thiol group (arrows show each event reaction); (b) proton transfer between −SH group and water (snapshots of b1, b2, and b3 are in time sequence); and (c) proton transfer between −SH group and carboxyl group (snapshots of c1, c2, and c3 are in time sequence). Atoms are colored: Au atoms: yellow; S atoms: red; H atoms: cyan; O atoms: blue; N atoms: purple; C atoms: green; water molecules: gray.

the simulation trajectories, proton transfer is detected. A thiol group (−SH), which is located away from the terminal bound on the NP surface, can deprotonate and transfer its proton to an oxygen atom of a neighboring water molecule (Figure 6b) or a carboxyl group of a peptide (Figure 6c). In the meantime, a deprotonated thiol group in a cysteine can also act as a hydrogen bond acceptor (Figure 6a). Our results of the proton transfer between thiol groups and water are consistent with the previous DFT simulations of the thiolate process.[74,75] The proton exchange between a thiol group and a carboxyl group is also in agreement with previous experimental results and DFT simulations.[76,77] It can be expected that the deprotonated thiol group can also serve as the initial state for subsequent possible

DOI: 10.1021/acs.langmuir.8b03951
Langmuir 2019, 35, 5029−5036

thiol−Au reactions, which can occur in the larger time scale of seconds[15] beyond the simulation scale in our current studies.

CONCLUSIONS

In this work, using ReaxFF MD simulations, we studied the peptide-grafted AuNPs by taking into account the complex interactions of thiols and polarizable atoms with gold nanoparticle surfaces, the amino acid residues' protonation state, and the steric effect of the SAMs. Our model system consists of AuNPs modified with short peptide chains composed of amino acid residues of cysteine and glycine. We compare different surface grafting densities of peptides to study their interactions with AuNPs. AuNPs of lower surface density were found to have more tight surface packing compared to the cases of higher density due to the steric effects near NP surfaces. Peptide atoms prefer to adsorb onto Au(111) facet rather than other facets of Au(110) and Au(100). Due to the thiol−Au bonding and the strong binding of polarizable oxygen and nitrogen atoms with gold surfaces, peptide chains are tightly adsorbed on AuNP surfaces. Moreover, the outer surfaces of the AuNP core are polarized with positive electrostatic potentials and atoms of inner core are negatively charged. However, at the outer layer of grafting, peptides consisting of amino acid residues of cysteine and glycine display negative electrostatic potentials. Furthermore, proton transfer from thiol groups of cysteine residues to water or carboxyl groups was detected over the course of simulation, which is in agreement with the quantum simulations and experiments in the previous literature. Longer simulations will be performed with more efficient RXMD in our future work.

ASSOCIATED CONTENT

Supporting Information

The Supporting Information is available free of charge on the ACS Publications website at DOI: 10.1021/acs.langmuir.8b03951.

Initial normalized surface coverages (α) for different facets (Figure S1); root-mean-square displacement (RMSD) for AuCGCG47 and AuCGCG72 in the last 100 ps (Figure S2); peptide density profile around AuNPs by averaging 100 configurations of the last 100 ps (Figure S3); coarse-grained simulation of AuCGCG (Figure S4) (PDF)

AUTHOR INFORMATION

Corresponding Author

*E-mail: tao.wei@howard.edu.

ORCID

Tao Wei: 0000-0001-6888-1658

Notes

The authors declare no competing financial interest.

ACKNOWLEDGMENTS

T.W. and A.Z.C. thank the support of grant from the National Science Foundation (NSF 1831559). T.W. is indebted to computational resources from the program of Extreme Science and Engineering Discovery Environment (XSEDE) and the Texas Advanced Computing Center (TACC). The authors thank Dr Aiichiro Nakano at the University of Southern California (USC) for the discussion of ReaxFF MD simulations and detailed instructions of the RXMD code provided by the Materials Genome Innovation for Computational Software (MAGICS) center at USC.

REFERENCES

(1) Balamurugan, B.; Maruyama, T. Evidence of an enhanced interband absorption in Au nanoparticles: size-dependent electronic structure and optical properties. *Appl. Phys. Lett.* **2005**, *87*, No. 143105.

(2) Shukla, R.; Bansal, V.; Chaudhary, M.; Basu, A.; Bhonde, R. R.; Sastry, M. Biocompatibility of gold nanoparticles and their endocytotic fate inside the cellular compartment: a microscopic overview. *Langmuir* **2005**, *21*, 10644−10654.

(3) Khlebtsov, N.; Dykman, L. Biodistribution and toxicity of engineered gold nanoparticles: a review of in vitro and in vivo studies. *Chem. Soc. Rev.* **2011**, *40*, 1647−1671.

(4) Kelly, K. L.; Coronado, E.; Zhao, L. L.; Schatz, G. C. The optical properties of metal nanoparticles: the influence of size, shape, and dielectric environment. *J. Phys. Chem. B* **2003**, *107*, 668−677.

(5) Storhoff, J. J.; Marla, S. S.; Bao, P.; Hagenow, S.; Mehta, H.; Lucas, A.; Garimella, V.; Patno, T.; Buckingham, W.; Cork, W.; et al. Gold nanoparticle-based detection of genomic DNA targets on microarrays using a novel optical detection system. *Biosens. Bioelectron.* **2004**, *19*, 875−883.

(6) El-Sayed, I. H.; Huang, X.; El-Sayed, M. A. Surface plasmon resonance scattering and absorption of anti-EGFR antibody conjugated gold nanoparticles in cancer diagnostics: applications in oral cancer. *Nano Lett.* **2005**, *5*, 829−834.

(7) Zhang, L.; Gu, F.; Chan, J.; Wang, A.; Langer, R.; Farokhzad, O. Nanoparticles in medicine: therapeutic applications and developments. *Clin. Pharmacol. Ther.* **2008**, *83*, 761−769.

(8) De Jong, W. H.; Borm, P. J. Drug delivery and nanoparticles: applications and hazards. *Int. J. Nanomed.* **2008**, *3*, No. 133.

(9) Pohjolainen, E.; Häkkinen, H.; Clayborne, A. The Role of the Anchor Atom in the Ligand of the Monolayer-Protected Au25 (XR) 18-Nanocluster. *J. Phys. Chem. C* **2015**, *119*, 9587−9594.

(10) Haes, A. J.; Van Duyne, R. P. A nanoscale optical biosensor: sensitivity and selectivity of an approach based on the localized surface plasmon resonance spectroscopy of triangular silver nanoparticles. *J. Am. Chem. Soc.* **2002**, *124*, 10596−10604.

(11) Demers, L. M.; Mirkin, C. A.; Mucic, R. C.; Reynolds, R. A.; Letsinger, R. L.; Elghanian, R.; Viswanadham, G. A fluorescence-based method for determining the surface coverage and hybridization efficiency of thiol-capped oligonucleotides bound to gold thin films and nanoparticles. *Anal. Chem.* **2000**, *72*, 5535−5541.

(12) Lévy, R.; Thanh, N. T.; Doty, R. C.; Hussain, I.; Nichols, R. J.; Schiffrin, D. J.; Brust, M.; Fernig, D. G. Rational and combinatorial design of peptide capping ligands for gold nanoparticles. *J. Am. Chem. Soc.* **2004**, *126*, 10076−10084.

(13) Ning, X.; Peng, C.; Li, E. S.; Xu, J.; Vinluan, R. D., III; Yu, M.; Zheng, J. Physiological stability and renal clearance of ultrasmall zwitterionic gold nanoparticles: Ligand length matters. *APL Mater.* **2017**, *5*, No. 053406.

(14) Scarì, G.; Porta, F.; Fascio, U.; Avvakumova, S.; Dal Santo, V.; De Simone, M.; Saviano, M.; Leone, M.; Del Gatto, A.; Pedone, C.; et al. Gold nanoparticles capped by a GC-containing peptide functionalized with an RGD motif for integrin targeting. *Bioconjugate Chem.* **2012**, *23*, 340−349.

(15) Xue, Y.; Li, X.; Li, H.; Zhang, W. Quantifying thiol−gold interactions towards the efficient strength control. *Nat. Commun.* **2014**, *5*, No. 4348.

(16) Krüger, D.; Fuchs, H.; Rousseau, R.; Marx, D.; Parrinello, M. Pulling monatomic gold wires with single molecules: an ab initio simulation. *Phys. Rev. Lett.* **2002**, *89*, No. 186402.

(17) Chen, F.; Li, X.; Hihath, J.; Huang, Z.; Tao, N. Effect of anchoring groups on single-molecule conductance: comparative study of thiol-, amine-, and carboxylic-acid-terminated molecules. *J. Am. Chem. Soc.* **2006**, *128*, 15874−15881.

DOI: 10.1021/acs.langmuir.8b03951
Langmuir 2019, 35, 5029−5036

(18) Harrison, E.; Hamilton, J. W.; Macias-Montero, M.; Dixon, D. Peptide functionalized gold nanoparticles: the influence of pH on binding efficiency. *Nanotechnology* **2017**, *28*, No. 295602.
(19) Heinz, H.; Farmer, B. L.; Pandey, R. B.; Slocik, J. M.; Patnaik, S. S.; Pachter, R.; Naik, R. R. Nature of molecular interactions of peptides with gold, palladium, and Pd−Au bimetal surfaces in aqueous solution. *J. Am. Chem. Soc.* **2009**, *131*, 9704−9714.
(20) Feng, J.; Pandey, R. B.; Berry, R. J.; Farmer, B. L.; Naik, R. R.; Heinz, H. Adsorption mechanism of single amino acid and surfactant molecules to Au {111} surfaces in aqueous solution: design rules for metal-binding molecules. *Soft Matter* **2011**, *7*, 2113−2120.
(21) Wei, T.; Ma, H.; Nakano, A. Decaheme Cytochrome MtrF Adsorption and Electron Transfer on Gold Surface. *J. Phys. Chem. Lett.* **2016**, *7*, 929−936.
(22) Wei, T.; Sajib, M. S. J.; Samieegohar, M.; Ma, H.; Shine, K. Self-Assembled Monolayers of an Azobenzene Derivative on Silica and Their Interactions with Lysozyme. *Langmuir* **2015**, *31*, 13543−13552.
(23) Samieegohar, M.; Ma, H.; Sha, F.; Sajib, M. S. J.; Guerrero-Garcia, G. I.; Wei, T. Understanding the interfacial behavior of lysozyme on Au (111) surfaces with multiscale simulations. *Appl. Phys. Lett.* **2017**, *110*, No. 073703.
(24) Wei, T.; Carignano, M. A.; Szleifer, I. Lysozyme Adsorption on Polyethylene Surfaces: Why Are Long Simulations Needed? *Langmuir* **2011**, *27*, 12074−12081.
(25) Wei, T.; Carignano, M. A.; Szleifer, I. Molecular Dynamics Simulation of Lysozyme Adsorption/Desorption on Hydrophobic Surfaces. *J. Phys. Chem. B* **2012**, *116*, 10189−10194.
(26) Zhang, T. T.; Wei, T.; Han, Y. Y.; Ma, H.; Samieegohar, M.; Chen, P. W.; Lian, I. A.; Lo, Y. H. Protein-Ligand Interaction Detection with a Novel Method of Transient Induced Molecular Electronic Spectroscopy (TIMES): Experimental and Theoretical Studies. *ACS Cent. Sci.* **2016**, *2*, 834−842.
(27) Nakano, C. M.; Ma, H.; Wei, T. Study of lysozyme mobility and binding free energy during adsorption on a graphene surface. *Appl. Phys. Lett.* **2015**, *106*, No. 153701.
(28) Mahmoudi, M.; Lynch, I.; Ejtehadi, M. R.; Monopoli, M. P.; Bombelli, F. B.; Laurent, S. Protein-Nanoparticle Interactions: Opportunities and Challenges. *Chem Rev.* **2011**, *111*, 5610−5637.
(29) Penna, M. J.; Mijajlovic, M.; Biggs, M. J. Molecular-Level Understanding of Protein Adsorption at the Interface between Water and a Strongly Interacting Uncharged Solid Surface. *J. Am. Chem. Soc.* **2014**, *136*, 5323−5331.
(30) Raffaini, G.; Ganazzoli, F. Protein Adsorption on a Hydrophobic Surface: A Molecular Dynamics Study of Lysozyme on Graphite. *Langmuir* **2010**, *26*, 5679−5689.
(31) Patwardhan, S. V.; Emami, F. S.; Berry, R. J.; Jones, S. E.; Naik, R. R.; Deschaume, O.; Heinz, H.; Perry, C. C. Chemistry of Aqueous Silica Nanoparticle Surfaces and the Mechanism of Selective Peptide Adsorption. *J. Am. Chem. Soc.* **2012**, *134*, 6244−6256.
(32) Shao, Q.; Hall, C. K. Binding Preferences of Amino Acids for Gold Nanoparticles: A Molecular Simulation Study. *Langmuir* **2016**, *32*, 7888−7896.
(33) Rechendorff, K.; Hovgaard, M. B.; Foss, M.; Zhdanov, V. P.; Besenbacher, F. Enhancement of protein adsorption induced by surface roughness. *Langmuir* **2006**, *22*, 10885−10888.
(34) Zhou, J.; Tsao, H. K.; Sheng, Y. J.; Jiang, S. Y. Monte Carlo simulations of antibody adsorption and orientation on charged surfaces. *J. Chem. Phys.* **2004**, *121*, 1050−1057.
(35) Shao, Q.; Hall, C. K. Protein adsorption on nanoparticles: model development using computer simulation. *J. Phys.: Condens. Matter* **2016**, *28*, No. 414019.
(36) Yang, J.; Wang, B.; You, Y. S.; Chang, W. J.; Tang, K.; Wang, Y. C.; Zhang, W. Z.; Ding, F.; Gunasekaran, S. Probing the modulated formation of gold nanoparticles-beta-lactoglobulin corona complexes and their applications. *Nanoscale* **2017**, *9*, 17758−17769.
(37) van Duin, A. C. T.; Dasgupta, S.; Lorant, F.; Goddard, W. A. ReaxFF: A reactive force field for hydrocarbons. *J. Phys. Chem. A* **2001**, *105*, 9396−9409.
(38) Liu, J.; Guo, X. ReaxFF molecular dynamics simulation of pyrolysis and combustion of pyridine. *Fuel Process. Technol.* **2017**, *161*, 107−115.
(39) Ashraf, C.; Jain, A.; Xuan, Y.; van Duin, A. C. T. ReaxFF based molecular dynamics simulations of ignition front propagation in hydrocarbon/oxygen mixtures under high temperature and pressure conditions. *Phys. Chem. Chem. Phys.* **2017**, *19*, 5004−5017.
(40) Sajib, M. S. J.; Sarnieegohar, M.; Wei, T.; Shing, K. Atomic-Level Simulation Study of n-Hexane Pyrolysis on Silicon Carbide Surfaces. *Langmuir* **2017**, *33*, 11102−11108.
(41) Cheng, X. M.; Wang, Q. D.; Li, J. Q.; Wang, J. B.; Li, X. Y. ReaxFF Molecular Dynamics Simulations of Oxidation of Toluene at High Temperatures. *J. Phys. Chem. A* **2012**, *116*, 9811−9818.
(42) Chenoweth, K.; Cheung, S.; van Duin, A. C. T.; Goddard, W. A.; Kober, E. M. Simulations on the thermal decomposition of a poly(dimethylsiloxane) polymer using the ReaxFF reactive force field. *J. Am. Chem. Soc.* **2005**, *127*, 7192−7202.
(43) van Duin, A. C. T.; Zeiri, Y.; Dubnikova, F.; Kosloff, R.; Goddard, W. A. Atomistic-scale simulations of the initial chemical events in the thermal initiation of triacetonetriperoxide. *J. Am. Chem. Soc.* **2005**, *127*, 11053−11062.
(44) Strachan, A.; Kober, E. M.; van Duin, A. C. T.; Oxgaard, J.; Goddard, W. A. Thermal decomposition of RDX from reactive molecular dynamics. *J. Chem. Phys.* **2005**, *122*, No. 054502.
(45) Newsome, D. A.; Sengupta, D.; Foroutan, H.; Russo, M. F.; van Duin, A. C. T. Oxidation of Silicon Carbide by O-2 and H2O: A ReaxFF Reactive Molecular Dynamics Study, Part I. *J. Phys. Chem. C* **2012**, *116*, 16111−16121.
(46) Nomura, K.; Kalia, R. K.; Li, Y.; Nakano, A.; Rajak, P.; Sheng, C. Y.; Shimamura, K.; Shimojo, F.; Vashishta, P. Nanocarbon synthesis by high-temperature oxidation of nanoparticles. *Sci. Rep.* **2016**, *6*, No. 24109.
(47) Senftle, T. P.; Hong, S.; Islam, M. M.; Kylasa, S. B.; Zheng, Y.; Shin, Y. K.; Junkermeier, C.; Engel-Herbert, R.; Janik, M. J.; Aktulga, H. M.; et al. The ReaxFF reactive force-field: development, applications and future directions. *npj Comput. Mater.* **2016**, *2*, No. 15011.
(48) Wu, Y. L.; Wang, C.; Zhao, J.; Cui, J. Y.; Yan, Y. S.; Li, C. X. Accelerating the design of gold/polymers/silica-based imprinted nanocomposite for light-triggered recognition and separation of biomolecules. *Chem. Eng. J.* **2017**, *307*, 621−630.
(49) Monti, S.; Carravetta, V.; Agren, H. Simulation of Gold Functionalization with Cysteine by Reactive Molecular Dynamics. *J. Phys. Chem. Lett.* **2016**, *7*, 272−276.
(50) Monti, S.; Carravetta, V.; Agren, H. Decoration of gold nanoparticles with cysteine in solution: reactive molecular dynamics simulations. *Nanoscale* **2016**, *8*, 12929−12938.
(51) Monti, S.; Carravetta, V.; Agren, H. Theoretical Study of the Adsorption Mechanism of Cystine on Au(110) in Aqueous Solution. *Small* **2016**, *12*, 6134−6143.
(52) Monti, S.; Carravetta, V.; Ågren, H. Simulation of gold functionalization with cysteine by reactive molecular dynamics. *J. Phys. Chem. Lett.* **2016**, *7*, 272−276.
(53) Chen, X.; Moore, J. E.; Zekarias, M.; Jensen, L. Atomistic electrodynamics simulations of bare and ligand-coated nanoparticles in the quantum size regime. *Nat. Commun.* **2015**, *6*, No. 8921.
(54) Zhu, Y.-X.; Jia, H.-R.; Pan, G.-Y.; Ulrich, N. W.; Chen, Z.; Wu, F.-G. Development of a Light-Controlled Nanoplatform for Direct Nuclear Delivery of Molecular and Nanoscale Materials. *J. Am. Chem. Soc.* **2018**, *140*, 4062−4070.
(55) Plimpton, S. Fast parallel algorithms for short-range molecular dynamics. *J. Comput. Phys.* **1995**, *117*, 1−19.
(56) Lustemberg, P.; Vericat, C.; Benitez, G.; Vela, M.; Tognalli, N.; Fainstein, A.; Martiarena, M.; Salvarezza, R. Spontaneously formed sulfur adlayers on gold in electrolyte solutions: Adsorbed sulfur or gold sulfide? *J. Phys. Chem. C* **2008**, *112*, 11394−11402.
(57) Berendsen, H. J.; Postma, J.; van Gunsteren, W. F.; DiNola, A.; Haak, J. Molecular dynamics with coupling to an external bath. *J. Chem. Phys.* **1984**, *81*, 3684−3690.

DOI: 10.1021/acs.langmuir.8b03951
Langmuir 2019, 35, 5029−5036

(58) Nakano, A. Parallel multilevel preconditioned conjugate-gradient approach to variable-charge molecular dynamics. *Comput. Phys. Commun.* **1997**, *104*, 59−69.
(59) Rappe, A. K.; Goddard, W. A., III Charge equilibration for molecular dynamics simulations. *J. Phys. Chem.* **1991**, *95*, 3358−3363.
(60) Monticelli, L.; Kandasamy, S. K.; Periole, X.; Larson, R. G.; Tieleman, D. P.; Marrink, S.-J. The MARTINI coarse-grained force field: extension to proteins. *J. Chem. Theory Comput.* **2008**, *4*, 819−834.
(61) Song, B.; Yuan, H.; Jameson, C. J.; Murad, S. Role of surface ligands in nanoparticle permeation through a model membrane: a coarse-grained molecular dynamics simulations study. *Mol. Phys.* **2012**, *110*, 2181−2195.
(62) Wright, L. B.; Palafox-Hernandez, J. P.; Rodger, P. M.; Corni, S.; Walsh, T. R. Facet selectivity in gold binding peptides: exploiting interfacial water structure. *Chem. Sci.* **2015**, *6*, 5204−5214.
(63) Ting, E. C.; Popa, T.; Paci, I. Surface-site reactivity in small-molecule adsorption: A theoretical study of thiol binding on multi-coordinated gold clusters. *Beilstein J. Nanotechnol.* **2016**, *7*, 53−61.
(64) Di Felice, R.; Selloni, A. Adsorption modes of cysteine on Au (111): Thiolate, amino-thiolate, disulfide. *J. Chem. Phys.* **2004**, *120*, 4906−4914.
(65) Abraham, A.; Ilott, A. J.; Miller, J.; Gullion, T. 1H MAS NMR Study of Cysteine-Coated Gold Nanoparticles. *J. Phys. Chem. B* **2012**, *116*, 7771−7775.
(66) Sandoval, A. P.; Orts, J. M.; Rodes, A.; Feliu, J. M. Adsorption of glycine on Au (hkl) and gold thin film electrodes: an in situ spectroelectrochemical study. *J. Phys. Chem. C* **2011**, *115*, 16439−16450.
(67) Samieegohar, M.; Ma, H.; Sha, F.; Jahan Sajib, M. S.; Guerrero-García, G. I.; Wei, T. Understanding the interfacial behavior of lysozyme on Au (111) surfaces with multiscale simulations. *Appl. Phys. Lett.* **2017**, *110*, No. 073703.
(68) Kenzler, S.; Schrenk, C.; Frojd, A. R.; Häkkinen, H.; Clayborne, A. Z.; Schnepf, A. Au 70 S 20 (PPh 3) 12: an intermediate sized metalloid gold cluster stabilized by the Au 4 S 4 ring motif and Au-PPh 3 groups. *Chem. Commun.* **2018**, *54*, 248−251.
(69) Weerawardene, K. D. M.; Häkkinen, H.; Aikens, C. M. Connections Between Theory and Experiment for Gold and Silver Nanoclusters. *Annu. Rev. Phys. Chem.* **2018**, *69*, 205−229.
(70) Liu, K.; Tiwari, S.; Sheng, C.; Krishnamoorthy, A.; Hong, S.; Rajak, P.; Kalia, R. K.; Nakano, A.; Nomura, K.; Vashishta, P.; Kunaseth, M.; Naserifar, S.; Goddard, W. A., III; Luo, Y.; Romero, N. A.; Shimojo, F. In *Shift-Collapse Acceleration of Generalized Polarizable Reactive Molecular Dynamics for Machine Learning-Assisted Computational Synthesis of Layered Materials*, 2018 IEEE/ACM 9th Workshop on Latest Advances in Scalable Algorithms for Large-Scale Systems, 2018.
(71) Verma, A.; Stellacci, F. Effect of surface properties on nanoparticle−cell interactions. *Small* **2010**, *6*, 12−21.
(72) Blanco, E.; Shen, H.; Ferrari, M. Principles of nanoparticle design for overcoming biological barriers to drug delivery. *Nat. Biotechnol.* **2015**, *33*, No. 941.
(73) Yao, C.; Wang, P.; Zhou, L.; Wang, R.; Li, X.; Zhao, D.; Zhang, F. Highly biocompatible zwitterionic phospholipids coated upconversion nanoparticles for efficient bioimaging. *Anal. Chem.* **2014**, *86*, 9749−9757.
(74) Sarangi, R.; Frank, P.; Benfatto, M.; Morante, S.; Minicozzi, V.; Hedman, B.; Hodgson, K. O. The x-ray absorption spectroscopy model of solvation about sulfur in aqueous L-cysteine. *J. Chem. Phys.* **2012**, *137*, No. 205103.
(75) Bachrach, S. M.; Nguyen, T. T.; Demoin, D. W. Microsolvation of cysteine: a density functional theory study. *J. Phys. Chem. A* **2009**, *113*, 6172−6181.
(76) DeBlase, A. F.; Kass, S. R.; Johnson, M. A. On the character of the cyclic ionic H-bond in cryogenically cooled deprotonated cysteine. *Phys. Chem. Chem. Phys.* **2014**, *16*, 4569−4575.
(77) Li, H.; Lin, Z.; Luo, Y. Gas-phase IR spectroscopy of deprotonated amino acids: Global or Local minima? *Chem. Phys. Lett.* **2014**, *598*, 86−90.

DOI: 10.1021/acs.langmuir.8b03951
Langmuir 2019, 35, 5029−5036